FIRE SUPPRESSION LBY PARTICULATES CONTAINING METALLIC COMPOUNDS

by

P.C. Wanigarathne, R.H. Krauss, H.K. Chelliah, R.J. and Davis, R.J.
University of Virginia

Reprinted from the Halon Options Technical Working Conference. Proceedings. HOTWC 2000. Sponsored by: University of New Mexico, Fire Suppression Systems Assoc., Fire and Safety Group, Great Lakes Chemical Corp., Halon Alternative Research Corp., Hughes Associates, Inc., Kidde Fenwal, Inc., Kidde International, Modular Protection, Inc., Next Generation Fire Suppression Technology Program, Sandia National Laboratories, Summit Environmental Corp., Inc. and 3M Specialty Materials. May 2-4, 2000, Albuquerque, NM, 2000.

NOTE: This paper is a contribution of the National Institute of Standards and Technology and is not subject to copyright.

NIST
National Institute of Standards and Technology
Technology Administration, U.S. Department of Commerce

FIRE SUPPRESSION BY PARTICULATES CONTAINING METALLIC COMPOUNDS

P.C. Wanigarathne, R.H. Krauss, H.K. Chelliah, R.J., and Davis, R.J.
University of Virginia

UNIVERSITY OF VIRGINIA INTRODUCTION

Fire suppression mechanisms by chemically active particulates (especially those due to alkali metal bicarbonates) have been investigated for a considerable period of time [1–4], but have received renewed interest because of the ban on production of Halon 1301 [5–9]. Some recent studies have indicated that on a mass basis, fine sodium bicarbonate ($NaHCO_3$) powder is about 2-10 times more effective in suppressing fires than the now banned Halon 1301, while iron pentacarbonyl vapor is known to be about 60 times more effective [10]. The exact chemical and physical models that describe the suppression mechanism of such compounds are not well established and development of a comprehensive method of testing these detailed models is the focus of the present investigation. This effort has been pursued along two paths, (a) model development effort based on relatively well studied sodium bicarbonate particles and (b) development of super effective fire suppressing particles, where a highly effective metallic compound (e.g., iron pentacarbonyl) is encapsulated in a porous solid particle (e.g., zeolite X). The details of these two efforts are described below.

FIRE SUPPRESSION WITH $NaHCO_3$

As mentioned above, fine $NaHCO_3$ powder (<10 μm) is known to be far more effective than any other gaseous chemical agent being considered to replace Halon 1301, but the exact physical and chemical mechanism of $NaHCO_3$ is yet to be quantified. Early studies with $NaHCO_3$ have hypothesized that the surface area of the particles plays a key role in determining its effectiveness. However, a recent experimental investigation by Trees and Seshadri [6] aimed at characterizing the particle size effects of $NaHCO_3$ has indicated a non-monotonic variation of particle mass fraction required to extinguish a flame as a function of the particle size (for the size range 0-30 μm). Although counterflow flame extinction experiments, similar to those in Trees and Seshadri [6], were performed by Fleming and co-workers [8, 9], to our knowledge, no attempt has been made to verify the above counter intuitive nonmonotonic size effects of $NaHCO_3$ for the size range of 0-30 μm. In addition, no detailed modeling effort has been undertaken to describe a physical mechanism for the existence of such a phenomenon. A better understanding of the underlying fire suppression mechanism of $NaHCO_3$ particles is expected not only to clarify the above results, but also assist future efforts on (a) development of new fire suppressants with superior chemical, thermal, and physical properties and (b) design of optimum delivery methods of such condensed phase agents.

When sodium bicarbonate particles are heated, they are known to decompose into oxides of Na in two stages. In the first stage, $NaHCO_3$ decomposes to solid sodium carbonate (Na_2CO_3), H_2O, and CO_2 around 543 K (note that the global decomposition temperature can vary depending on the particle heating rate, e.g., smaller particles are expected to heat rapidly when exposed to the flame environment because of their higher surface area/volume ratios than the larger particles). In the second stage, Na_2CO_3 formed is known to decompose at 1170 K, leading to formation of Na_2O and CO_2. In the presence of water, however, Na_2CO_3 and Na_2O are known to react to form sodium hydroxide (NaOH) [2]. The NaOH formed promotes catalytic recombination of the

radicals species needed for flame propagation, causing the flame to extinguish readily [11]. The present experimental and theoretical study was undertaken to address uncertainties regarding effect of sodium bicarbonate particle size on flame extinction, and more importantly, to develop a rigorous method of quantifying various physical, thermal, and chemical contributions.

EXPERIMENTS WITH $NaHCO_3$

In the present flame extinction experiments, a counterflow of nonpremixed methane and air with a steady laminar flame established within the mixing layer is considered (Figure 1). The sodium bicarbonate particles, which were separated into size ranges of <10, 10-20, 20-30, 30-40, and 40-60 μm using a vortex separation technique, are introduced with the air stream at a relatively steady rate. Obtaining a steady particle feed rate and its calibration have been the most challenging aspect of the present experimental investigation. Typical particle mass fraction introduced with the air stream was about 1%, corresponding to a particle flow rate of about 0.1 gm/min. For a selected sodium bicarbonate loading, the flame extinction effectiveness of sodium bicarbonate particles was characterized by the extinction flow strain rate, measured by two methods (a) global formula based on the nozzle exit velocities and nozzle separation distance [12] and (b) local velocity field measurements using laser Doppler velocimetry (LDV).

PARTICLE SEEDER

Because of the need to establish the accuracy of previously reported data with $NaHCO_3$ particles considerable attention was devoted to the development of a particle seeder that could deliver steady feed rates of particles of various sizes (i.e., from 0 to 100 μm). For small airflow rates involved (typical flow rates of 0.1 liter/s), the fluidized bed approach shown in Figure 1 gave satisfactory seeder performance only for relatively small particles, i.e., less than 30 μm. This fluidized bed seeder consists of a 19 mm diameter glass tube with two porous plugs connected at either end using Swagelock fittings. The air inflow to the seeder, controlled through a mass flow controller, was split into two streams and connected to either end of the glass tube. The flow passing through the bottom, which controls the fluidization level, was monitored through another flow controller. The fluidized particles and the total air entering the fluidization tube were ejected through a small tube located towards the middle of the tube. By maintaining the total air flowing through the fluidizer tube constant, the mass fraction of particles was expected to attain steady state. The particle feed rate was continuously monitored using a Mie scattering detection system located at the exit of the seeder air (Figure 1). This detection system consists of a laser diode operating at 671 nm, a Thor Labs DET1-SI High Speed Silicon Detector with collection by a 3-cm focal length lens, background radiation filtering using an Edmund Scientific 671 nm interference filter, and a Hewlett-Packard Model 7132 strip chart recorder. Because the seeder air flow rate was held fixed, scattering signal was independent of the total air flow rate exiting through the air nozzle and was primarily dependent on the particle delivery rate of the seeder. The scattered signal was observed to decay slightly over 20-30 min periods, but could be controlled by shifting part of the bottom fluidizing air to the top. Different particle flow rates were obtained by controlling the fraction of seeder air flowing through the top and the bottom. The actual mass fraction of the particles in the air stream was determined by calibrating the recorded scattering signal by a separate gravimetric analysis, usually performed before and after each flame extinction experiment.

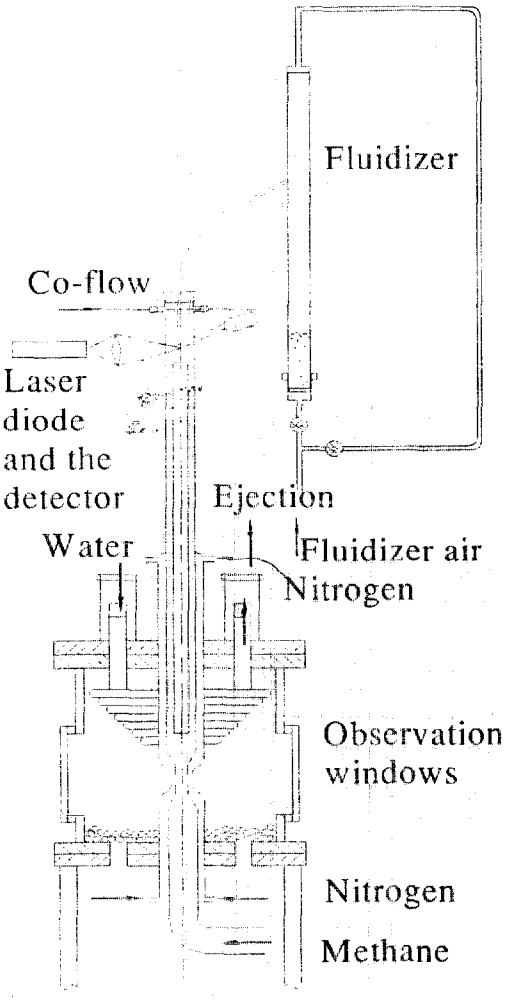

Figure 1. Schematic of the experimental configuration, with the particle seeder.

For particles greater than 20 μm, a positive feed auger system (not shown) was employed. This seeder arrangement consisted of a multi-start Teflon screw (diameter of 7 mm OD and 5 mm ID) in a high-precision stainless steel tube where the screw was driven by speed-locked variable speed motor. This seeder was vibrated pneumatically to assist the particle flow, but the particle feed rate was primarily controlled by the motor rpm. Part of the total airflow was diverted through a screw-driven particle seeder and then mixed with the remaining air prior to exiting through the air nozzle. As before, airflow through the seeder held constant while the total air-flow through the nozzle was varied to attain different flame strain rates. For particle sizes above 20 μm, the seeder described above performed extremely well with variation of the Mie scattering signal less than +/- 10%. In this positive feed auger system, particles below 20 μm had a tend-ency to clump, and consequently significant variation of the scattering signal was observed. To overcome such clumping, in the previous work by Hamins et al. [5], about 1\% by mass of 10 nm silica particles had been added to the sodium bicarbonate particles. Because of the uncertainty of the effect of adding such fine silica particles and also the associated safety issues, this approach was not pursued here.

MEASURED FLAME EXTINCTION RESULTS

In counterflow flame experiments, the flame extinction condition can be directly related to the extinction flow strain rate (which is related to the axial velocity gradient along the axis of symmetry) and is typically reported based on (a) global strain rate formula derived by Seshadri and Williams [12], or (b) local velocity gradients along the axis of symmetry measured using LDV. For the methane and air nonpremixed flames considered, without particles, the measured global flame extinction strain rate was about 470 s^{-1}, while the measured local LDV strain rate was about 390 s^{-1}. These values are consistent with those reported previously by Chelliah et al. [13]. As sodium bicarbonate particles are added to the air stream, the flame extinction strain rate is expected to decrease because of the physical, thermal, and chemical effects of the particles. For different particle size groups (<10,10-20, 20-30, 30-40 and 40-60 μm), using the particle seeders developed, the measured variation of flame extinction strain rate vs. the sodium bicarbonate particle mass fraction in the air stream is shown in Figure 2. All particle size groups demonstrated a clear decrease in the extinction strain with increasing particle loading. For a given particle mass fraction, 10-20 μm particles indicate the lowest extinction strain rate indicating its higher effectiveness as a suppressant.

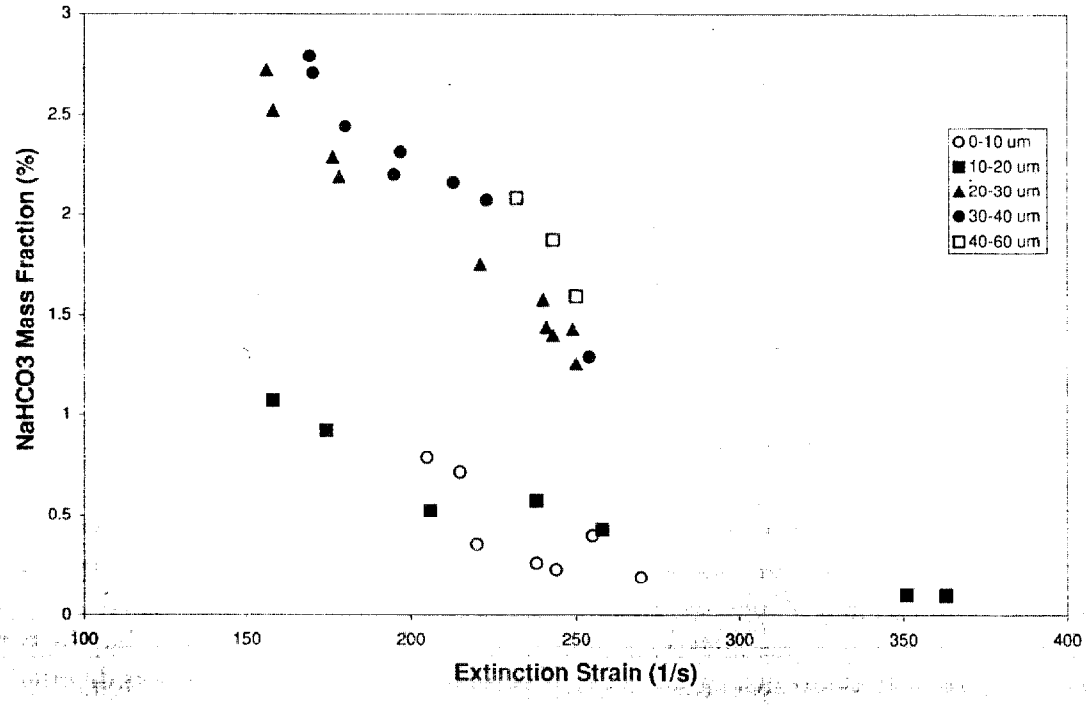

Figure 2. Comparison of the sodium bicarbonate mass fraction as a function of extinction strain rate, for different size groups of particles.

Seshadri and co-workers [5, 6] have previously reported a similar trend in variation of the mass of particle required with varying extinction strain rate, for each size group. However, between size groups, they observed non-monotonic effectiveness, namely 0-10 μm the most effective, 10-20 μm the least effective, and 20-30 μm with an intermediate effectiveness. It should be pointed out that there are a few key differences in the two studies. For example, the fuels used were different and could have an impact on the results (in Trees and Sheshadri [6] a liquid heptane fuel pool was used, while in the present experiments gas methane was used). Second, in

Seshadri's experiments, about 1% by mass of 10 nm silica particles was added to minimize the clumping of particles and help fluidize the smaller particles considered. Although experiments were performed in the present system using 0-10 μm particles without addition of silica particles, the particle feed rate fluctuations were too large (~ +/-30%) with potential inaccuracies of the particle feed rate calibrations.

NUMERICAL SIMULATION OF $NaHCO_3$ PARTICLE EFFECTS

A numerical model, based on a hybrid Eulerian-Lagrangian formulation for the gas and condensed phase, has been developed recently to describe the interaction of fine-water droplets with counterflow nonpremixed laminar flames and its extinction phenomena [14]. This model was extended to include the effects of $NaHCO_3$ particle transport, heating, decomposition, and subsequent interaction of decomposed gaseous species with the homogeneous flame chemistry. The detailed gas-phase kinetic model for methane-air was augmented with a 20-step elementary mechanism for Na from Jensen and Jones [11]. Although there are considerable uncertainties in the global particle decomposition model, the theoretical approaches are expected to provide detailed information about the rate controlling physical, thermal, and chemical effects of $NaHCO_3$ particles.

$NaHCO_3$ DECOMPOSITION MODEL

Unlike the analysis of fire suppression by water droplets, the model developed for $NaHCO_3$ particles involves considerable uncertainties. These include the non-spherical nature of the particles, the transient heating effect of the particles, the heterogeneous decomposition mechanism of $NaHCO_3$, and the gas-phase chemical inhibition mechanism by intermediate species formed.

Previous studies have indicated that sodium bicarbonate decomposes at a low temperature of about 543 K to form sodium carbonate through the reaction [1]

$$2\,(NaHCO_3)_s \rightarrow (Na_2CO)_s + CO_2 + H_2O.$$

For particle temperatures above 1124 K, the sodium carbonate formed can decompose further to form other reaction intermediates of Na. Based on these observations, Friedman and Levy [2] had postulated that NaOH is the primary inhibiting compound responsible for flame extinction and proposed the following reaction pathways leading to formation of NaOH

$$(Na_2CO_3)_s \rightarrow (Na_2O)_{liq} + CO_2,$$

$$(Na_2O)_{liq} + H_2O \rightarrow 2NaOH,$$

or

$$(Na_2O)_{liq} \rightarrow Na_2O,$$

followed by the homogeneous reaction

$$Na_2O + H_2O \rightarrow 2NaOH.$$

Once the alkali hydroxide is formed, the following catalytic radical scavenging cycle is known to be responsible for reduction of the radical pool

$$NaOH + H \rightarrow H_2O + Na,$$

$$Na + OH + M \rightarrow NaOH + M,$$

$$NaOH + OH \rightarrow H_2O + NaO.$$

The relative importance of these reactions is not well established and the literature indicates some conflicting results [2, 4, 9, 11].

In the initial simulations presented here, a fast global decomposition reaction of the form,

$$2(NaHCO_3)_s \rightarrow 2NaOH + 2CO_2$$

is employed here. The particle temperature at which the decomposition occurs (defined here as T_{decomp}) is varied to obtain the sensitivity of the particle size. Although such a global model can be fine tuned to a very narrow range of conditions, e.g., for a narrow particle size range, it should be cautioned here that extension of such models to a wider range of conditions may lead to physically unrealistic results. For the homogeneous chemistry associated with NaOH, a detailed reaction model involving 6 species in 20 elementary reactions proposed by Jensen and Jones [11] was employed, in conjunction with the detailed chemistry model for methane oxidation [14].

PREDICTED FLAME EXTINCTION RESULTS

Figure 3 shows the predicted variation of $NaHCO_3$ mass fraction as a function of flame extinction strain rate, for selected sodium bicarbonate particle size groups with mass fraction of 1% in the air stream. For comparison, a plot of equivalent NaOH mass fraction for different extinction strain rates is also shown. The predicted curve with NaOH indicates the absolute maximum inhibition possible, based on the homogeneous model employed. Different NaOH reaction mechanisms are expected to modify this curve, but the predicted trends are not expected to change. The results clearly indicate that particles above 20 μm have a small effect on flame extinction, but as the particle size decreases below 20 μm, the extinction strain rate decreases significantly, indicating a remarkable increase in the effectiveness. This effect is attributed to the rapid heating of the particle and fast decomposition process.

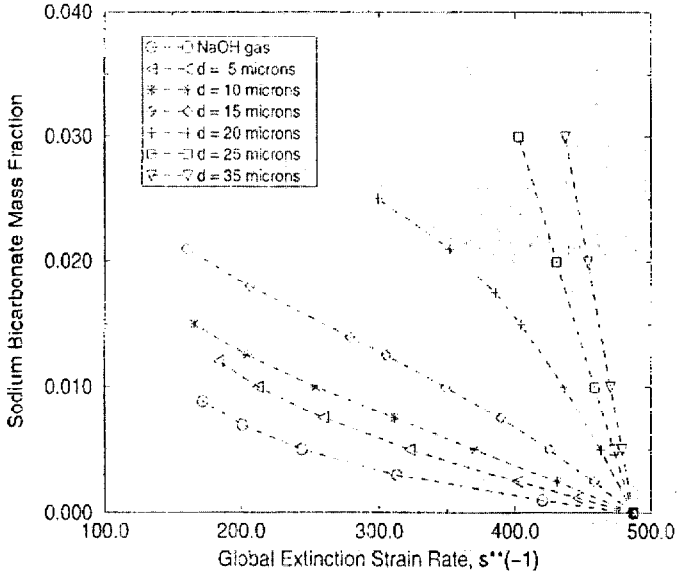

Figure 3. Numerical prediction of sodium bicarbonate mass fraction as a function of extinction strain rate, for selected sizes of particles.

By varying the T_{decomp} described earlier, the location at which these particles are rapidly decomposing in the flow field can be varied. As a consequence, the amount of Na released to the homogeneous phase is affected, leading to a varying degree of chemical inhibition. To quantify the contributing thermal and chemical effects, the source terms can be selectively turned "off" in the model. Unlike previously reported fine-water droplet simulations, these results indicate a significant chemical effect in the presence of $NaHCO_3$. For dilute particle loading considered here, the physical effects are found to be negligible. Methods of improving the particle heating and subsequent heterogeneous particle decomposition models are currently being analyzed and such efforts are expected to provide far more accurate flame extinction results.

ENCAPSULATION OF $Fe(CO)_5$

Iron pentacarbonyl, $Fe(CO)_5$, known to be one of the most effective fire suppression compounds, is extremely toxic and flammable [15,16]. Hence, direct utilization of $Fe(CO)_5$ in fire suppression applications is impractical. However, an extremely effective fire suppressing compound can be developed if this toxic compound can be encapsulated or immobilized in a benign solid matrix (or support material), from which it can be released when exposed to the high temperature region of a flame front. Because of our previous experience in developing and working with zeolite compounds, the encapsulation of $Fe(CO)_5$ in zeolite was considered first in this investigation.

ABSORPTION METHOD

Figure 4 shows a schematic of the absorption/impregnation setup. Two glass tubes were connected to a vacuum pump, capable of achieving pressure of 50 mtorr. In the initial absorption studies, about 1 gm of solid support material was first inserted into one of the tubes. This sample was then heated under vacuum conditions to remove the absorbed gases from the internal pore structure, which typically took about 3-4 hours. After removal of the absorbed gases, the support material was allowed to return to room temperature. The $Fe(CO)_5$ to be absorbed was then poured into the second tube, with the interconnecting valve closed. While keeping the $Fe(CO)_5$ close to freezing temperature, the valve in the interconnecting tube was opened briefly to remove the gas-$Fe(CO)_5$ mixture. Finally, the valve to the suction pump was closed and the interconnecting tube valve opened, allowing the $Fe(CO)_5$ vapor to diffuse and absorb into the pore structure. This vapor-phase absorption process typically took about 1-2 days. At the end of the absorption process, zeolite particles were observed to change to a faint brown/yellow color. Based on the change in color of zeolite, the absorption was observed to be uniform across the entire sample.

When $Fe(CO)_5$ absorbed zeolite was exposed to air, a rapid propagation of a reaction front across the sample is observed. To determine the effect of oxygen concentration on the decomposition/oxidation process, separate experiments were conducted by exposing the encapsulated zeolite-X particles to pure oxygen. The latter investigation has indicated a dramatic increase in the decomposition process. Since $Fe(CO)_5$ is also known to decompose readily when exposed to light, several investigations were performed with different light intensities. Besides the physical factors indicated above, the surface properties of the support material can have an important role in the $Fe(CO)_5$ decomposition process. Experiments were conducted with zeolite-Y and silica particles with mesopores to address this issue. The basic difference between zeolite-X and zeolite-Y is in the content of Na in the solid matrix. The $Fe(CO)_5$ absorbed zeolite-Y also indicated similar $Fe(CO)_5$ decomposition characteristics when exposed to air, but the intensity of

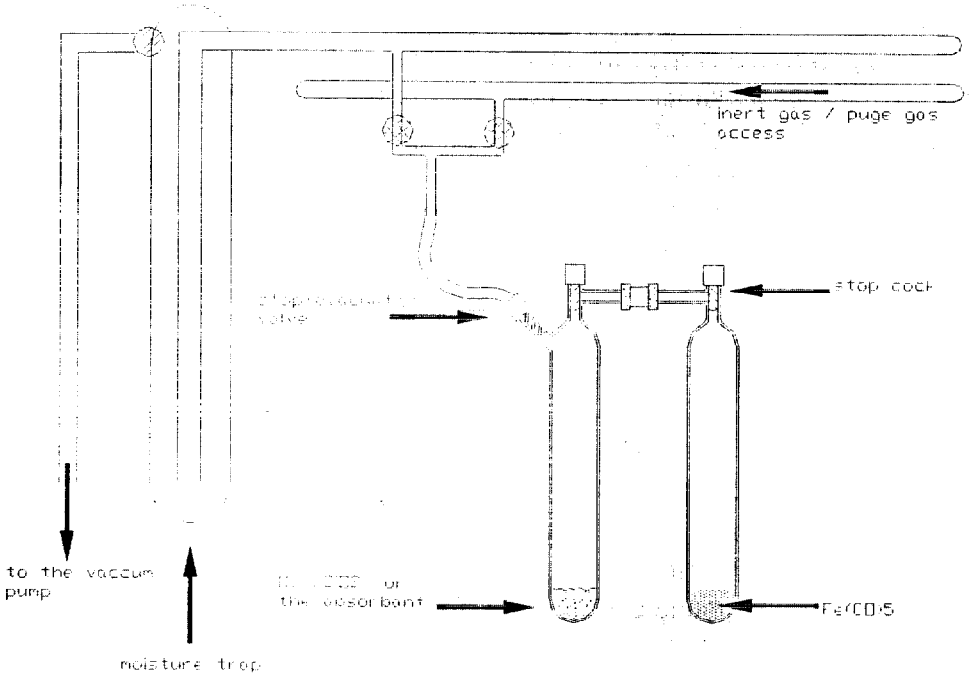

Figure 4. Schematic of the $Fe(CO)_5$ absorption method.

the observed reaction rate is much slower than in zeolite-X. In contrast, porous silica particles gave no visible indications of $Fe(CO)_5$ decomposition.

Because of the breakdown of $Fe(CO)_5$ within the pore structure of zeolite, TGA analysis with absorbed zeolite could not be performed. Instead, elemental analyses (performed by Southern Testing & Research Laboratories, Inc.) of $Fe(CO)_5$ encapsulated particles have revealed very interesting information about the level of Fe absorption (Table 1).

TABLE 1. SUMMARY OF THE ELEMENTAL ANALYSIS.

Support Material	Na mass fraction (%)	Fe mass fraction (%)
Zeolite-X	10.6	8.85
Zeolite-Y	6.79	9.71
SiO_3	<0.8	12.8

As seen in Table 1, both zeolite X and Y have a significant amount of Na embedded in their structure. The absorbed iron mass fraction is also significant and comparable to the Na loading. Considering the superior fire suppression ability of Fe (which is about 5-25 times more effective than Na), these particles may show a superior fire suppression ability. The exact size of condensed iron or oxides of iron is not known yet, but high-resolution microscopic studies to be undertaken shortly will clarify this issue. Premixed flame studies with these dissociated $Fe(CO)_5$ in zeolite will be conducted in the near future to quantify the effectiveness of these encapsulated particles. The motivation for switching to premixed flame suppression studies is its simplicity, and more importantly, safety issues associated with $Fe(CO)_5$.

CONCLUSIONS

The goal of the present investigation was (a) to develop a comprehensive model that can identify the leading mechanism of fire suppression of sodium bicarbonate particles and (b) to investigate the concept of developing super effective iron pentacarbonyl encapsulated particles.

Designing a steady particle seeder for sizes ranging from 0-60 μm proved to be a rather challenging task. Two independent approaches of particle seeding were developed for the size range considered, and the flame extinction experiments indicated that both approaches yielded identical results for the overlapping particle size range of 20-30 μm, providing considerable confidence in the measured results. All the particle sizes considered (i.e., <0,10-20, 20-30, and 40-60 μm) indicated a decrease in flame extinction strain rate with increasing particle mass fraction, a result consistent with previous work. However, the effectiveness of flame suppression (quantified here based on the amount of $NaHCO_3$ mass fraction needed) is shown to vary monotonically with particle size, with the smallest size group being the most effective.

Numerical predictions performed taking into account the detailed homogeneous chemistry and global particle decomposition model indicate a trend in particle effectiveness very similar to that obtained from the experiments. By varying the temperature at which the particles decompose rapidly to gaseous products, the predictions have shown that the smallest particles are more effective because of the rapid heating, leading to complete decomposition of the particles. By manipulating various source terms in the model, the superior effectiveness of sodium bicarbonate particles was attributed to the homogeneous catalytic radical scavenging by NaOH formed, while thermal effects associated with particle heating play a minor role.

Results with iron pentacarbonyl encapsulated in porous zeolite particles indicate that $Fe(CO)_5$ is not stable and reacts when exposed to air/oxygen. The elemental analysis performed indicates that the Fe mass fraction in zeolite is about 10% by mass. The effectiveness of these dissociated $Fe(CO)_5$ absorbed zeolite particles will be tested in the near future using a premixed flame setup.

ACKNOWLEDGMENTS

This work was supported by National Institute of Standards and Technology, Gaithersburg, MD.

REFERENCES

1. Dolan, J.E., and Dempster, P.B., "The Suppression of Methane-Air Ignition by Fine Powders," *J. Appl. Chem.* 5, p. 510, 1955.
2. Friedman, R., and Levy, J.B., "Inhibition of Opposed-Jet Methane-Air Diffusion Flames: the Effects of Alkali Metal Vapors and Organic Halides," *Combustion and Flame* 7:195, 1963.
3. Birchall, J.D., "On the Mechanism of Flame Inhibition by Alkali Metal Salts," *Combustion and Flame* 14:85, 1970.
4. McHale, E.T., "Flame Inhibition by Potassium Compounds," *Combustion and Flame*, 24:277, 1975.

5. Hamins, A., Gmurczyk, G., Grosshandler, W., Presser, C., and Seshadri, K., "Flame Suppression Effectiveness," *Evaluation of Alternate In-Flight Fire Suppressants for Full-Scale Testing in Aircraft Engine Nacelles and Dry Bays*, W.L. Grosshandler, R.G. Gann, and W.M. Pitts (eds.), NIST SP-861, April 1994.

6. Trees, D., and Seshadri, K., "Experimental Studies of Flame Extinction by Sodium Bicarbonate ($NaHCO_3$) Powder," *Combust. Sci. and Tech.* 122:215, 1997.

7. Hamins, A., "Flame Extinction by Sodium Bicarbonate Powder in a Cup Burner," Twenty-Seventh Symposium, Int. on Combustion, The Combustion Institute, pp. 2857-2864, 1998.

8. Fleming, J.W., Reed, E.J.P, Zegers, E.J.P, Williams, B.A., and Sheinson, R.S., "Extinction Studies of Propane/Air Counterflow Flames: The Effectiveness of Aerosols," *Proceedings*, Halon Options Technical Working Conference, Albuquerque, NM, pp. 333-342, 1998.

9. Williams, B.A., and Fleming, J.W., "Suppression Mechanisms of Alkali Metal Compounds," *Proceedings*, Halon Options Technical Working Conference, Albuquerque, NM, pp. 157-169, 1999.

10. Babushok, V., Tsang, T., Linteris, G.T., and Reinelt, D., "Chemical Limits to Flame Inhibition," *Combustion and Flame* 115, 551-560, 1998,

11. Jensen, D.E., and Jones, G.A., "Kinetics of Flame Inhibition by Sodium," *J. Chem. Soc.*, Faraday Trans. Part I 78, p. 2843, 1982.

12. Seshadri, K., and Williams, F.A., "Laminar Flow Between Parallel Plates with Injection of a Reactant at High Reynolds Number," *Int. J. Heat Mass Transfer* 21: 251-253, 1978.

13. Chelliah, H.K, Law, C.K., Ueda, T., Smooke, M.D., and Williams, F.A., "An Experimental and Theoretical Investigation of Flow-Field, Dilution and Pressure Effects on the Extinction Condition of Methane/Oxygen/Nitrogen Diffusion Flames," *Proceedings of the Twenty-third Symposium, Int. on Combustion*, The Combustion Institute, pp. 503-511, 1990.

14. Lentati, A.M., and Chelliah, H.K., "Dynamics of Water Droplets in a Counterflow Field and Their Effect on Flame Extinction," *Combustion and Flame* 115:158-179, 1998.

15. Lask, G., and Wagner, H.G., "Influence of Additives on the Velocity of Laminar Flames," *Proc. Combust. Inst.*, 8, p. 432, 1962.

16. Reinelt, D., and Linteris, G.T., "Experimental Study of the Inhibition of Premixed and Diffusion Flames by Iron Pentacarbonyl." *Twenty-sixth Symposium*, Int. on Combustion, The Combustion Institute, pp. 1421-1428, 1996.